PAPER

Gold nanoparticle superlattices as functional solids for concomitant conductivity and SERS tuning†

Edakkattuparambil Sidharth Shibu,[a] Jobin Cyriac,[ab] Thalappil Pradeep*[a] and J. Chakrabarti*[c]

Mercaptosuccinic acid protected gold nanoparticles (Au@MSA) self assemble to form superlattice (SL) crystals at the air–water interface. These have been used for gas adsorption. The current–voltage (I–V) characteristics of the SL film with embedded SL crystals, obtained by four probe measurements, show Ohmic conduction. The conductance observed was proportional to the polarizability of the adsorbed gases. The current through the SL decreases on adsorption of the gas along with decrease in the SERS intensity of a probe molecule from the crystals. We rationalise our observation of the linear dependence of the conductance on the polarizability of the adsorbed gas using a simple model calculation. Variation of the conductance may be useful in designing electrical switches operating at the nanometre length scales.

Introduction

One of the fastest developing areas in nanotechnology over the last several years is the fabrication of well defined two or three dimensional (2D or 3D) nanoparticle superlattices (SLs). Since the creation of 3D assemblies of semiconducting quantum dots (QD),[1] manipulation of such hierarchical self-assemblies to create enhanced and tunable quantum confinement effects has been an active research area.[2] These structures may be called "artificial solids"[1] which belong to a new class of materials and open up a variety of applications in solar cells,[3] light emitting diodes,[4] molecular electronic architectures,[5] high-density data storage,[6] catalysis,[7] biochemical sensors,[8] bio-compatible materials,[9] *etc.*

Gold nanoparticle SLs are distinctly different from corresponding QD systems. When grown at air–water interfaces, SL crystals of tens of micrometres in dimension are formed with interesting morphologies.[10,11] These SL crystals are embedded on SL films which float at the air–water interfaces and can be scooped out for examination. New functionalities such as fluorescence[12] can be introduced in such materials. Such induced

functionalities can be harnessed for a variety of applications, including the detection of biomolecules[13] and size dependent[14,15] and temperature dependent[16] electrical charge transport, to name a few. Recently, we reported a rapid method for the fabrication of mercaptosuccinic acid protected gold nanoparticle super-lattices (Au@MSA SLs) under N_2 gas flow.[17] Hydrogen bonding between the adjacent ligands in nanoparticles builds up a network of channels in the crystal. The constituent nano-particles in these types of SLs follow fcc stacking along with nanometre voids. Further, the superlattice provides rough and porous surfaces due to the periodic long range order of constituent particles spanning over micrometres, and thus can act as an excellent platform for surface enhanced Raman scattering (SERS) studies.[17] We reported Raman imaging of a single Au@MSA SL crystal which showed more enhancement of the Raman intensity from the edges than from the flat surfaces due to the enhanced electric field at the former regions.[17] There are several experimental and theoretical results dealing with the transport properties of nanoparticle arrays.[18–29]

The porous structure of Au@MSA SL can be utilized to tune various properties of the SL crystal. For instance, the SL has a highly inhomogeneous dielectric property: It is a periodic arrangement of metallic nanoparticles, embedded in a network of ligand molecules of very low dielectric constant along with ample void spaces. The electrical polarization in the presence of an external electric bias can be tuned, if the void spaces are filled up with guest molecules. The polarization in the medium would affect the transport of a charge carrier and thus the electrical conductance in the SL. The SERS intensity should reflect the changes in the local polarization. With this backdrop, we focus here on the simultaneous changes in the electrical transport and SERS of an Au@MSA SL crystal due to the presence of adsorbed gases in the voids. We perform four probe measurements of

[a] DST Unit on Nanoscience (DST UNS), Department of Chemistry and Sophisticated Analytical Instrument Facility, Indian Institute of Technology, Madras, Chennai, 600 036, India
[b] The Aston Labs for Mass Spectrometry, Department of Chemistry, Purdue University, West Lafayette, IN 47907, USA
[c] S. N. Bose National Centre for Basic Sciences, Block-JD, Sector-III, Salt Lake, Kolkata, 700091, India. E-mail: pradeep@iitm.ac.in; Fax: +91-44 2257-0545; jaydeb@bose.res.in

† Electronic supplementary information (ESI) available: **(1)** Optical image of SL crystals sitting on the surface of four probe electrodes and photograph of the electrode. **(2)** Change in Raman spectrum with applied potential. **(3)** The conductance change of all gases at 0.5 volt (100 and 500 Torr exposure). See DOI: 10.1039/c0nr00670j.

the I–V characteristics and find that the conduction is Ohmic and is proportional to the polarizability of the adsorbed gas. We substantiate the coupling between the polarization field and the conductance by observing decrease in the SERS intensities on exposure to gases for a given bias voltage across the sample. Further, we show that the current through the SL can be controlled by exposure to gases due to changes in the conductance. All these changes are brought about reversibly. Finally, we calculate *via* simple electrostatics[30] the changes in the polarization of the medium in the presence of adsorbed gas atoms/molecules to rationalize the qualitative features of the changes in conductance. We thus provide a molecular level understanding for the measured SL conductance, paving the way to control the electrical transport properties of the SL which is essential for different applications.

Experimental

Materials

All the chemicals were commercially available and used without further purification. $HAuCl_4 \cdot 3H_2O$, methanol (GR grade) and ethanol (GR grade) were purchased from SRL Chemical Co. Ltd, India. $NaBH_4$ (>90%) and mercaptosuccinic acid (MSA, M. W. = 106) were from Sigma Aldrich. Deionized (DI) water of resistivity > 18 MΩ cm was used for all the experiments.

Synthesis of Au@MSA

Au@MSA nanoparticles were synthesized using a reported protocol[17] with a few modifications. To a 50 mL methanolic solution (5 mM) of $HAuCl_4 \cdot 3H_2O$, 5 mM MSA was added (1 : 1 ratio, total volume of methanol was 200 mL). The mixture was cooled to 0 °C in an ice bath for 30 min. Then, an aqueous solution of $NaBH_4$ (0.2 M, 50 mL), cooled to 0 °C, was injected rapidly into the above mixture under vigorous stirring. The mixture was allowed to react for another hour. The resulting precipitate was collected and washed repeatedly with methanol through centrifugal precipitation. Finally, the Au@MSA precipitate was dried and collected as a dark brown powder. Synthesis of Au@MSA SLs was done using our reported protocol.[17]

Sample characterization

The samples have been characterized by different physical techniques. High resolution transmission electron microscopy (HRTEM) images have been collected using JEOL 3010 UHR instrument. The samples were observed at 200 keV to reduce electron beam induced damage. Scanning electron microscopy (SEM) and energy dispersive analysis of X-rays (EDAX) were carried out with a FEI QUANTA 200 instrument.

Electrical measurements

Electrodes were fabricated on a silicon wafer by mask-assisted chemical vapour deposition of gold (four probes). Electrical leads were fixed onto gold pads using silver paste (SPI Supplies Inc). The SL film, scooped out from the air–water interface, was placed over the electrode with four probes spaced at ~70

micrometres. Several SL crystals of ~5 micrometre edge length are embedded on a typical SL film. The entire electrode set-up was kept in a glass tube with a vacuum seal. The current response before and after the exposure of gas at constant voltage was monitored using a Keithley 2700 digital multimeter-data acquisition system. The entire assembly is shown in Scheme 1. The I–V characteristics were studied using the four probe method. Gases were admitted through the gas line shown in the schematic and pressures were monitored through a manometer. A constant probe voltage, ranging from 0.0 to 2.0 V, was applied across the contacts labelled A and B by adjusting the probe tips in the desired direction and the current was measured across the other two contacts C and D at constant temperature (room temperature). An optical image of SL crystals sitting on the surface of the four probe electrode is given in the electronic supplementary information (Fig. S1†). A photograph of an entire electrode is also shown (inset of Fig. S1†). The current through several SL crystals and the extended SL film is measured in this set-up. In the experiment, we measured current not potential, as we considered the possibility of using such materials for hand-held applications using battery sources.

Raman measurements

All the SERS measurements were done using crystal violet (CV) as the Raman marker molecule. The CV solutions were prepared in water at 10^{-5} M concentrations. The electrode containing the SLs was dipped in the CV solution of required concentration for one hour. It was washed carefully three times with distilled water and dried under ambient conditions and was used for Raman measurements. This procedure results in the uniform coating of CV over SL films and ensured that excess molecules, if any, were washed away. After this, the electrical leads were fixed onto gold pads using silver paste (SPI Supplies Inc). The Raman spectrum and corresponding imaging have been done using a Witec GmbH confocal Raman spectrometer equipped with a 532 nm source with a spot size <1 μm. The laser has a maximum power of 40 mW. The excitation laser was focused using a 100× objective and the signal was collected in a back-scattered geometry and guided to a Peltier-cooled charge coupled device (CCD) detector. The sample was mounted on a piezo-equipped scan stage to enable spectral imaging. All data presented throughout the manuscript are collected from the same electrode and same sample. Moreover, we have repeated the same set of experiments several times to ensure the reproducibility of the experimental set-up and the device. We have successfully obtained the same results more than five times in each crystal investigated. To ensure reproducibility in SERS measurements, we choose a SL crystal and capture an optical image at the specific location. After each Raman measurement, the position of the SL crystal was rechecked using the optical microscope. In such cases the data points are comparable. Original spectra were recovered at the end of the experiments ensuring stability of the Raman probe.

Results and discussion

We present below the most essential characteristics of the SL crystals. Detailed analysis of these are presented elsewhere.[12,13,17]
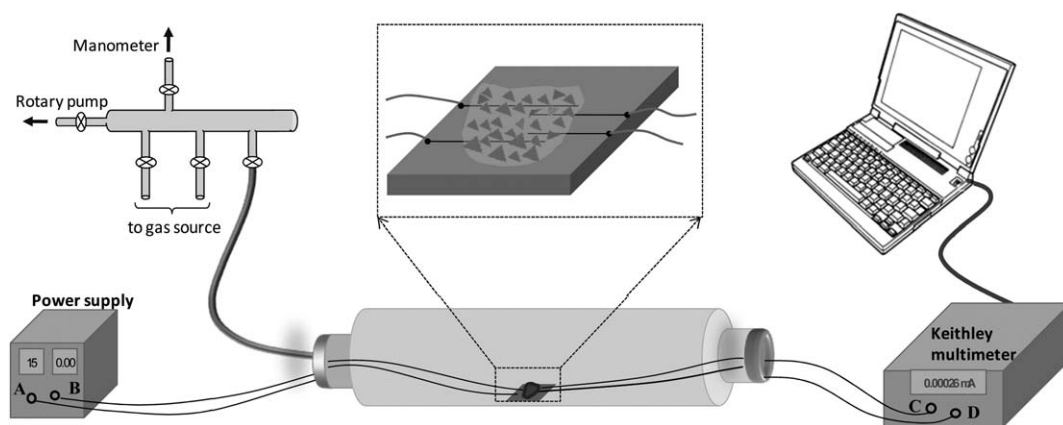
Scheme 1 Representation of the set-up used for measuring *I–V* characteristics of SLs. Triangles shown are SLs.

Fig. 1A shows a large area SEM image of SL crystals prepared from monodisperse truncated octahedral particles of ∼8.5 nm in diameter, showing several triangular morphologies. The SL crystals, marked with circles, are placed over an SL film. Arrangement of the nanoparticles in the SL film, analyzed by HRTEM, shows cubic close packing with an interparticle spacing of 10.4 nm (inset a1 in Fig. 1A). The same arrangement exists in the crystal also. The electron beam transmission is adequate only at the edges of the crystal and the lattice is clearly visible there. In the images, a $[110]_{SL}$ projection of the unit cell of the SL is represented by a rectangular box, where the subscript SL indicates the reflections from the SL. The particles are of
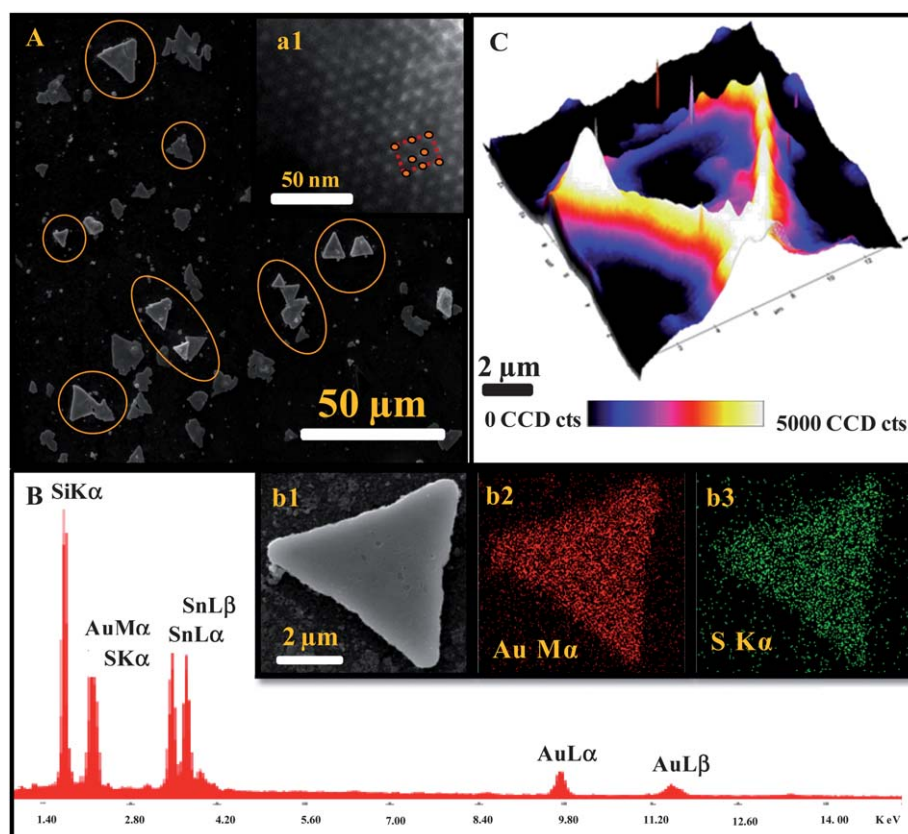

Fig. 1 (A) Large area SEM image of Au@MSA SLs embedded on an SL film. Inset (a1) shows HRTEM image of the edge of a SL crystal showing the periodic arrangement of nanoparticles with an inter-particle distance of 10.4 nm. $[110]_{SL}$ projection of the unit cell of the SL is represented by a rectangular box, where the subscript SL indicates the reflections from the SL. (B) The EDAX spectrum of SL crystal is shown in Fig. 1B. Si and Sn lines are due to the ITO substrate used for SEM/EDAX imaging. The corresponding EDAX maps of the same triangle using Au Mα and S Kα are given in insets (b2 and b3). (C) The color coded Raman image of SL crystal collected from an area of 12 μm × 12 μm using the intensities of CV features in the 200 to 2000 cm^{-1} window.

8.5 nm core diameter and, considering a length of 0.7 nm for the MSA monolayer, the effective diameter of the particle including the monolayer is ~9.2 nm. This suggests that there are tetrahedral and octahedral voids of 1.0 and 1.9 nm radii, respectively. These pores are adequate to accommodate small molecules. Stacking of the nanoparticles in the 3D superlattices has been characterized by small angle X-ray scattering (SAXS), which is reported elsewhere.[17] The constituent gold nanoparticles are stacked in a fcc pattern rather than hcp. The inter-planar spacing for (111) and (220) of Au@MSA SL are 10.5 and 6.4 nm, respectively, which is in good agreement with the HRTEM data, as mentioned above. The spatial distribution of gold in the SL film was analyzed by elemental mapping of a single crystal using energy dispersive analysis of X-rays (EDAX). Fig. 1B shows the EDAX spectrum collected from the triangular SL, shown in Fig. 1B-b1. EDAX mapping has been done using Au Mα, and S Kα and the images are shown in Fig. 1B-b2 and b3. The SL crystals are Raman active[17] and SERS from them was used to obtain corresponding Raman images. The Raman image of a single crystal (of ~7 μm edge length) is shown in Fig. 1C. The integration time used for imaging was 0.04 s and the area imaged was 12 μm $\times$ 12 μm. In this image, yellow regions have maximum Raman intensity and black regions have minimum intensity. The SERS intensity of the SL crystals is different at edges and surfaces due to the difference in the enhancement of electric field at these locations.[17]

We measured the I–V characteristics of the SL samples upon exposure to different gases at 500 torr. The I–V characteristics (Fig. 2) show a linear response for all the four gases (O_2, Ar, N_2 and CO_2). Details of the response for all the gases are given in a log-log plot in Fig. 2A. The log-log plots show a slope of nearly 1.0 ensuring a linear dependence of I on V. The linear response ensures Ohmic conduction in the system, the slope of the I–V trace being the conductance. The polarizability values of all the gases used for the experiments are given in the table (inset in Fig. 2B). The conductance vs. polarizability of the gas is shown in Fig. 2B. This clearly indicates that the conductance decreases linearly with the polarizability of the adsorbed gases.

The SERS intensity should show sensitivity to the polarization induced by different adsorbed gases. To this end, we performed SERS studies of Au@MSA SL crystals at two different pressures, namely 500 and 100 Torr of CO_2, using CV as an analyte at a bias voltage of 1.5 V. The data in Fig. 3A show a decrease in intensity of Raman signals with gas pressure. Clearly, at 10^{-2} Torr (vacuum), there is no CO_2 gas for adsorption and hence SERS intensity from the SL crystals is high. But upon exposing the SL crystals to the gas, the SERS intensity decreases with gas pressure and time; the drop in Raman intensity is more substantial at 500 Torr. The change in intensity follows the reverse trend upon evacuation of the set-up as well. Thus, gas exposure and consequent change in SERS is reversible. Note that the Raman peak positions show no change. We collect the time dependent SERS from the same crystals under 500 Torr CO_2 with exposure time; the data are given in Fig. 3B. The Raman spectral intensity changes with time and a steady intensity is observed after 800 s. We measured the Raman spectra under 500 Torr of different gases and plotted the Raman intensity of the 1170 cm^{-1} peak at the steady value vs. polarizability of the gases (Fig. 3C). The repeated exposures of gases and complete
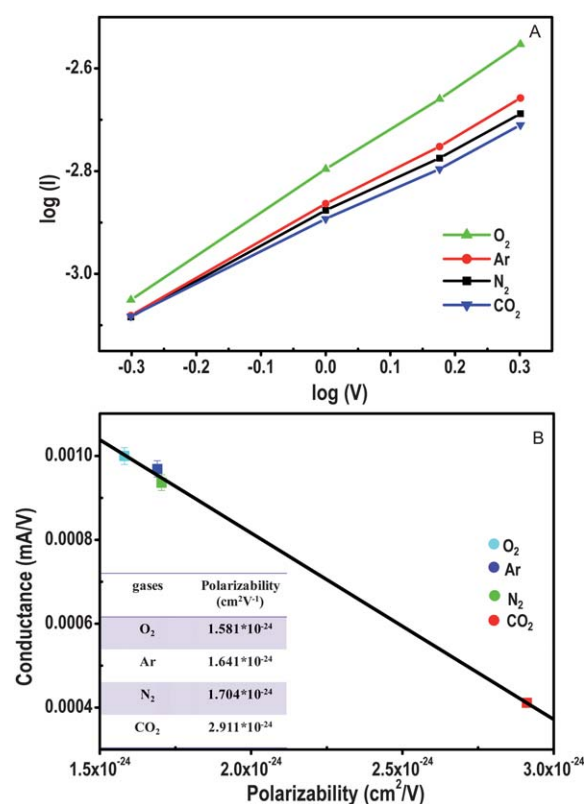

Fig. 2 (A) Plot of log current (mA) vs. log voltage (V) of the SL crystals upon exposure to gases, O_2, Ar, N_2, and CO_2 at 500 torr. (B) Conductance (slope of I vs. V, in mA V^{-1}) vs. polarizability (cm^2 V^{-1}) of the corresponding gases. Table in the inset shows the polarizability of all the four gases under consideration.

reversibility of signal suggest that there is nothing significantly changing with the CV-nanoparticle interaction. If there were substantial effects on the interactions as a result of gas molecules, some of the CV molecules may have desorbed and that would have caused some change in the Raman intensity. As this has not happened, we believe that no change has occurred near the particles. Several measurements have been conducted on the same crystals over extended periods, spread over several days, and no measurable change was seen. All the changes are instantaneous and completely reversible. All of these point to a screening effect and not a change in the nature of adsorption of CV. The plot shows that the intensity decreases linearly with polarizability of adsorbed gases, following the same trend as the conductance. We also observed some sensitivity of the Raman intensities to the applied potential (data given in electronic supplementary information, Fig. S2†).

The change in conductance under gas adsorption implies that current through the SL can be controlled by exposing it to gases. The current upon exposure to different gases, at a given pressure, is shown in Fig. 4A for an applied potential of 1.5 V. SLs were initially maintained in vacuum and a were then exposed to a series of gases at a pressure of 100 Torr and at a potential of 1.5 V, over several cycles with an exposure time of 5 min per cycle (Fig. 4A). The set-up was evacuated again for 5 min and then exposed to gas repeatedly. We find a small drop in the current upon gas exposure. However, the current does not seem to
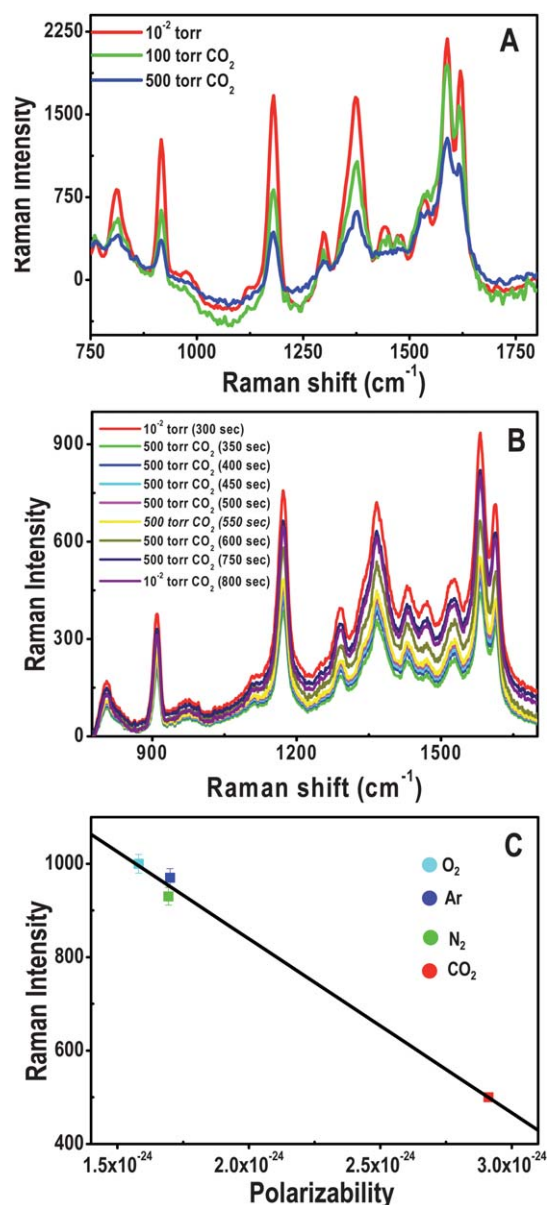
Fig. 3 (A) SERS spectrum collected at different concentrations of CO_2. (B) Change in SERS intensity of Au@MSA SL crystals under 500 Torr of CO_2 at different time intervals. (C) Change in Raman intensity *vs.* polarizability of gases at 500 Torr (O_2, Ar, N_2 and CO_2).

saturate with exposure time. The same experiment was conducted with 500 Torr for all the gases. The current drops substantially within a very short time ($\sim$10 s), eventually reaching a steady value, the magnitude being dependent on the gas. This steady state value obtained at 500 Torr is used in Fig. 2A. The current drops more for CO_2 than for other gases, the sequence being carbon dioxide, nitrogen, argon and oxygen, as can be seen in the data in Fig. 4B. Raman spectra of adsorbed CV were measured simultaneously as the current was monitored. The variation in the spectral intensity for the peak at 1170 cm^{-1} and current follow the same trend as shown in Fig. 4C. In the Figure, the Raman intensities have been scaled to bring them to the same range as the current. Similar responses were found for the other bands too. This observation clearly establishes that

changes in the polarization in the crystal that leads to the variation in the SERS intensity causes the observed effects in the electrical conductance as well. At a low voltage (0.5 V), the response was very poor for all the gases and the data are given in the ESI (Fig. S3†).

Theory

Simple electrostatics[30] gives insight into the experimental observations. Let us calculate how the polarization in the medium is affected by that of the adsorbed gases. We consider for simplicity a situation, schematically shown in Fig. 4D, where a unit cell consists of a metal sphere of diameter a, representing a gold nanoparticle which is surrounded by a coating of monolayer of spatial extent l, followed by adsorbed gas molecules of diameter d. The schematic diagram in Fig. 4D does not represent the actual number of the adsorbed molecules. The electrodes are infinitely removed along the z-axis, generating a uniform external electric field, E_0 parallel to the z-axis. The polarization of the monolayer protected gold nanoparticles is given by $a^3 \varepsilon_C[(\varepsilon_N - \varepsilon_C)/(\varepsilon_N + 2\varepsilon_C)]E_0$; ε_N and ε_C are the dielectric constants of the nanoparticle and the monolayer chains. For a metal, the dielectric constant can be taken to diverge, $\varepsilon_N \gg \varepsilon_C$ (ref. 30), in which case the polarization dipole due to the metal sphere is simply given by $(a^3 \varepsilon_c/2)E_0$. The polarization is large for spheres of a few nanometres in size. The polarization field modifies the local field in the system. The electric field at a point (r, $\ominus$) is given by E(r, $\ominus$) = $E_0 \cos(\ominus)(1 - a^3 \varepsilon_c/2r^3)$. The gas molecule adsorbed in the system is polarized by this modified electric field. Let us consider the situation close to the z-axis for simplicity. The polarized dipole moment of the adsorbed molecule produces an extra electric field that opposes this local electric field, and is given by p = αE_{pol} where E_{pol} is the polarization field, E at $r = a/2 + l + d/2$. We set cos ($\ominus$) = 1 for the electric field along the z-axis. α is the polarizability of the gas molecule. Considering the contribution due to the polarizations of n such adsorbed molecules in the vicinity of the nanoparticle, we get the net electric field given by $E_{net} = E(r = z, \ominus = 0) - 3np\varepsilon c/[z^3(2 + \varepsilon c)]$. The second term is due to the extra polarization of the adsorbed molecules that opposes the existing electric field and is proportional to the polarizability of the adsorbed molecule. This term can be appreciable due to a couple of factors: (1) The term depends on the local polarization field which could be large for nanometre sized particles. (2) It depends on n, which in turn depends on the density of the adsorbed molecules and the volume of the porous region. The density of the adsorbed molecules is given by the fugacity of the adsorbed molecules in the pore which must be the same in equilibrium as that in the reservoir where from adsorption takes places, the latter being proportional to the pressure. Note that n can be large for large pressures and large porous volumes. These two factors make the additional polarization due to the adsorbed molecules not negligible compared to the local field due to the capped metal nanoparticles. The net field E_{net} is appreciable to overcome the thermal motion of the charged carrier to result in the drift velocity $\nu = -eE_{net}/\gamma$, γ being the damping coefficient in the medium. Note that the drift velocity is proportional to E_0, implying Ohmic conduction of the charge, the proportionality factor being the conductance. Several qualitative features are noteworthy: (1) The conductance decreases
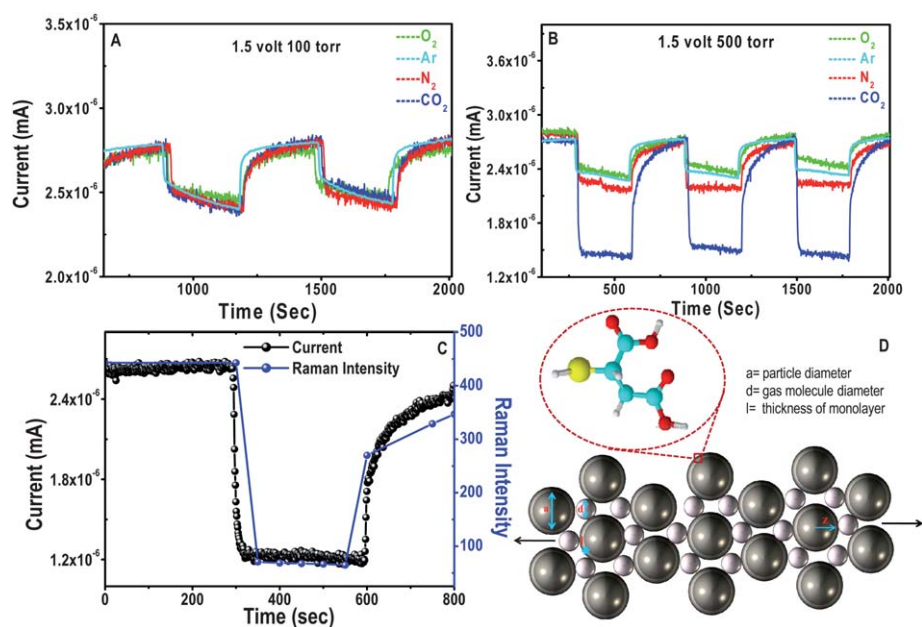
Fig. 4 Conductance changes of SLs (1.5 V) under the exposure of (A) 100 Torr and (B) 500 Torr of O_2, Ar, N_2 and CO_2, respectively. (C) Comparison of change in Raman intensity of the 1170 cm^{-1} band and current upon exposure to 500 Torr CO_2, performed simultaneously. The Raman intensities have been scaled so that the data points are comparable with current and on the same scale. (D) Cartoon representation of gas molecules adsorbed on the surface of nanoparticles in SLs.

due to the polarization of the adsorbed gas, the decrease being proportional to α, as observed in the experiments. (2) The local electric field E_{net} depends on n. n could be determined from the adsorption isotherm at a given chemical potential. One expects n to increase with the external pressure, implying that the change in conductance would be larger for a larger pressure. The change in current in the experiments is significant at higher gas pressures (500 Torr). At lower exposures (100 Torr) we find that there is significant variation of current with the time of exposure. This suggests that there could be additional factors responsible for the current response at lower exposures, which may be occupancy of different sites, diffusion in the lattice, *etc.* (3) The Raman intensity depends on the local electric field, E_{net}. Thus the change in the Raman intensity with pressure and different gases can be understood from the variation of E_{net} with α and n.

Conclusions

We have shown that the conductance of Au@MSA SL crystals is sensitive to adsorption of gases. The conductance, obtained from the *I–V* characteristics *via* four probe measurements, is proportional to the polarization of the adsorbed gases. The change in conductance is reflected in the change in current and its coupling to the polarization of the medium is demonstrated by the changes in the SERS intensity. The proportionality between the conductance and the polarization has been rationalized on the basis of simple electrostatic calculations where the charge carrier upon biasing experiences the polarization fields of different constituents of the system. The change in conductance with polarization of the adsorbed gas may be useful in finding new applications of such artificial solids. Direct measurement of the incorporation of molecules by Raman spectra of the probe molecules and their sensitivity to very small pressure variations is

interesting. This may prove Raman spectroscopy as a sensitive tool for gases which are not by themselves Raman active. As nanoparticle dimension can be varied with proper choice of the core and the monolayer shell, solids with variable pore sizes may be created allowing sensing and detection of specific gases.

References

1 C. B. Murray, C. R. Kagan and M. G. Bawendi, *Science*, 1995, **270**, 1335–1338.
2 C. P. Collier, T. Vossmeyer and J. R. Heath, *Annu. Rev. Phys. Chem.*, 1998, **49**, 371–404.
3 I. Gur, N. A. Fromer, M. L. Geier and A. P. Alivisatos, *Science*, 2005, **310**, 462–465.
4 M. Achermann, M. A. Petruska, S. Kos, D. L. Smith, D. D. Koleske and V. I. Klimov, *Nature*, 2004, **429**, 642–646.
5 S. A. Maier, P. G. Kik, H. A. Atwater, S. Meltzer, E. Harel, B. E. Koel and A. A. Reguicha, *Nat. Mater.*, 2003, **2**, 229–232.
6 J. Hoinville, A. Bewick, D. Gleeson, R. Jones, O. Kasyutich, E. Mayes, A. Nartowski, B. Warne, J. Wiggins and K. Wong, *J. Appl. Phys.*, 2003, **93**, 7187–7189.
7 J. Grunes, J. Zhu, E. A. Anderson and G. A. Somorjai, *J. Phys. Chem. B*, 2002, **106**, 11463–11468.
8 K. Motesharei and D. C. Myles, *J. Am. Chem. Soc.*, 1998, **120**, 7328–7336.
9 J. Spinke, M. Liley, H.-J. Guder, J. Angermaier and W. Knoll, *Langmuir*, 1993, **9**, 1821–1825.

10 H. Yao, T. Minami, A. Hori, M. Koma and K. Kimura, *J. Phys. Chem. B*, 2006, **110**, 14040–14045.

11 Y. Yang, S. Liu and K. Kimura, *Angew. Chem., Int. Ed.*, 2006, **45**, 5662–5665.

12 N. Nishida, N. E. S. Shibu, H. Yao, T. Oonishi, K. Kimura and T. Pradeep, *Adv. Mater.*, 2008, **20**, 4719–4723.

13 E. S. Shibu, M. A. H. Muhammed, K. Kimura and T. Pradeep, *Nano Res.*, 2009, **2**, 220–234.

14 A. S. Nair and K. Kimura, *J. Chem. Phys.*, 2008, **129**, 184117–184123.

15 A. S. Nair and K. Kimura, *Langmuir*, 2009, **25**, 1750–1756.

16 A. S. Nair and K. Kimura, *Phys. Chem. Chem. Phys.*, 2009, **11**, 9346–9350.

17 E. S. Shibu, K. Kimura and T. Pradeep, *Chem. Mater.*, 2009, **21**, 3773–3781.

18 D. Greshnykh, A. Frömsdorf, H. Weller and C. Klinke, *Nano Lett.*, 2009, **9**, 473–478.

19 U. Simon, *Adv. Mater.*, 1998, **10**, 1487–1492.

20 C. T. Black, C. B. Murray, R. L. Sandstrom and S. Sun, *Science*, 2000, **290**, 1131–1134.

21 M. P. J. Van Staveren, H. B. Brom and L. De Jongh, *Phys. Rep.*, 1991, **208**, 1–96.

22 R. H. Terrill, T. A. Postlethwaite, C. Chen, C. Poon, A. Terzis, A. Chen, J. E. Hutchison, M. R. Clark, G. Wignall, J. D. Londono, R. Superfine, M. Falvo, J. C. S. Johnson, E. T. Samulski and R. W. Murray, *J. Am. Chem. Soc.*, 1995, **117**, 12537–12548.

23 B. L. Altshuler, P. A. Lee, R. A. Webb, *Mesoscopic Phenomena in Solids*, North-Holland Publishing Co, Amsterdam, 1991.

24 D. L. Peng, K. Sumiyama, T. J. Konno, T. Hihara and S. Yamamuro, *Phys. Rev. B: Condens. Matter Mater. Phys.*, 1999, **60**, 2093–2100.

25 K. C. Beverly, J. L. Sample, J. F. Sampaio, F. Remacle, J. R. Heath and R. D. Levine, *Proc. Natl. Acad. Sci. U. S. A.*, 2002, **99**, 6456–6459.

26 P. Beecher, A. J. Quinn, E. V. Shevchenko, H. Weller and G. Redmond, *J. Phys. Chem. B*, 2004, **108**, 9564–9567.

27 A. A. Middelton and N. S. Wingreen, *Phys. Rev. Lett.*, 1993, **71**, 3198–3201.

28 A. J. Quinn, M. Biancardo, L. Floyd, M. Belloni, P. R. Ashton, J. A. Preece, C. A. Bignozzi and G. Redmond, *J. Mater. Chem.*, 2005, **15**, 4403–4407.

29 A. Quinn, P. Beecher, D. Iacopino, L. Floyd, G. De Marzi, E. Shevchenko, H. Weller and G. Redmond, *Small*, 2005, **1**, 613–618.

30 J. D. Jackson, *Classical Electrodynamics*, Wiley Eastern Ltd, New Delhi, 1982.